LANDMINE DETECTION USING THE DISCRETE SPECTRUM OF RELAXATION FREQUENCIES

Mu-Hsin Wei, Waymond R. Scott, Jr., and James H. McClellan

Georgia Institute of Technology
School of Electrical and Computer Engineering
777 Atlantic Drive NW, Atlanta, GA 30332-0250

ABSTRACT

Several landmine detection techniques using electromagnetic induction (EMI) sensors have been proposed in the past decade. In this paper, we propose a class of detection techniques based on the discrete spectrum of relaxation frequencies (DSRF). Two DSRF detection methods are demonstrated: one using the support vector machine and one using the k-nearest neighbor method. A soil model is also proposed to identify EMI response from the magnetic properties of the soil. A detection framework is suggested to incorporate the soil model and the classifier. The robustness of landmine detection using the DSRF is demonstrated.
Approved for public release; distribution is unlimited.

Index Terms— Electromagnetic induction (EMI), discrete spectrum of relaxation frequencies (DSRF), detection, support vector machine.

1. INTRODUCTION

Landmine detection techniques based on EMI sensors have been actively developed in the past decade. Gao *et al.* suggested a Bayesian classification algorithm which uses the frequency response of targets as a feature [1]. Fails *et al.* [2] and Ramachandran *et al.* [3] both demonstrated success in detecting mines using nearest-neighbor classifiers based on an EMI model developed by Miller *et al.* [4].

We propose to detect landmines using an EMI model based on the discrete relaxations of the target [5]. This model has several attractive features, including a sound theoretical treatment, physical significance of model parameters, and orientation invariance. The EMI frequency response of a metallic object can be expressed as a sum:

$$H(\omega) = c_0 + \sum_{k=1}^{L} \frac{c_k}{1 + j\omega/\zeta_k}, \qquad (1)$$

where c_0 is the shift, L the model order, c_k the real spectral amplitudes, and ζ_k the relaxation frequencies. The parameter set $S = \{(\zeta_k, c_k) : k = 1 \dots L\}$ is the DSRF. The DSRF of a target can be estimated using methods proposed in [6, 7].

The relaxation frequencies are invariant to the orientation and position of the target; only the spectral amplitudes change when the target is rotated or moved [5]. Therefore, the ζ_k can be used as a feature that is intrinsic to a target. Furthermore, since most landmines are buried in consistent orientations, the c_k are also often similar among different mines of the same type. Figure 1 demonstrates the consistency of the DSRF across instances of two different types of landmine [6]. While consistent within its own type, the two mines clearly have distinct DSRFs.

We propose to detect landmines using the DSRF as a feature. We propose two landmine classification methods: one based on the support vector machine (SVM) and one based on the k-nearest neighbor (kNN). A soil presecreener is also proposed. We suggest a detection framework that incorporates the proposed DSRF classifier and the soil prescreener. The resulting performance is robust and comparable to existing methods. The detection process is also very fast when using the SVM.

2. DETECTION METHODS

2.1. Target Classifier

We propose to classify a target based on its DSRF using the kNN or the SVM. With only two classes, landmine and not-landmine, the classification problem reduces to a detection problem.

In the case of kNN, the distance measure used to quantify the distance between two DSRFs is the Earth Mover's Distance (EMD) [8, 6]. The Euclidean distance is a poor measure of the similarity between the two DSRF because the relaxations of two DSRFs are usually sparse and not aligned. However, the EMD can account for the difference in the number of relaxations as well as when the relaxations are not aligned.

In the case of SVM, given a target's DSRF parameter set S, the target is classified/labeled using the decision function:

$$f(S) = sign\left(\sum_{i=1} \alpha_i y_i K(S_T^i, S) + b\right), \qquad (2)$$

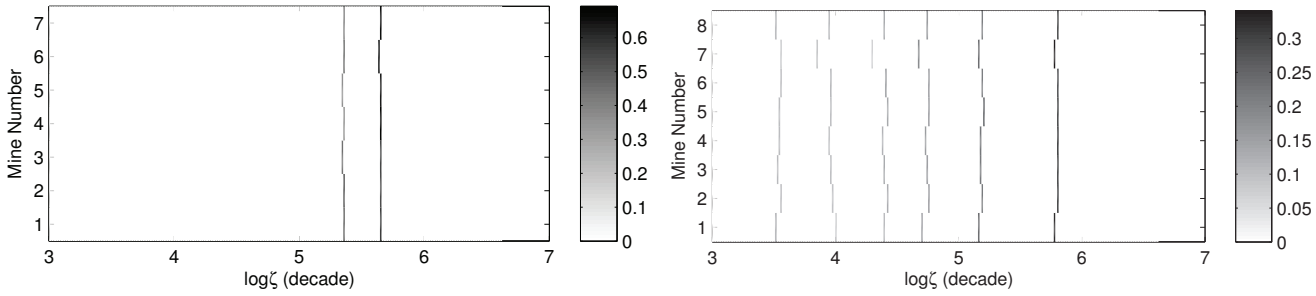

(a) (b)

Fig. 1. Estimated DSRF of landmines. The spectral amplitude c_k is represented by the intensity: the darker the color, the larger the amplitude. (a) Seven low-metal content, nonmagnetic, moderate EMI response antipersonnel mines. (b) Eight medium-metal content, magnetic, strong EMI response antipersonnel mines.

where K is the kernel (explained shortly), S_T^i the training data, $y_i \in \{-1, +1\}$ the training class labels, α_i the trained weights, and b the trained threshold. (Only a few αs are nonzero, i.e., the αs are sparse. The S_T^i that correspond to the nonzero α_i are called the *support vectors*.)

For the kernel, we use a generalized radial basis function [9]:

$$K_{\mathrm{EMD}}(S_1, S_2) = \exp(-\rho\,\mathrm{EMD}(S_1, S_2)), \qquad (3)$$

where ρ is a scaling parameter. For brevity, (3) is called the EMD kernel [10]. While it is not proven that the EMD kernel satisfies Mercer's condition (i.e., K_{EMD} is positive semi-definite), it is observed that the EMD kernel is positive semi-definite [10] in practice. At the least, it should be noted that kernels that do not satisfy Mercer's condition can still perform well [9].

2.2. Soil Prescreener

A soil model and a prescreener based on this model is presented here. The prescreener filters out responses that are like those due to the magnetic properties of the soil. The prescreening process is very efficient.

The frequency dependence of the soil responses share a similar trend. The real part has a linear trend with respect to the log-frequency, and the imaginary tends to be a constant [11, 12]. From these observations, we propose a model:

$$H_G(\omega) = p_1 + p_2\left(\ln\omega + j\frac{\pi}{2}\right), \qquad (4)$$

where $p1$ and $p2$ are model parameters. Given a response measured at N frequencies $\omega_1, \ldots, \omega_N$, the response can be fitted to the model (4) via a least-squares minimization, which can be performed very efficiently.

The responses for 6000 samples collected at locations that reported to have no metal content are shown in Fig. 2. Some magnitudes are strong (> -125 dB) because metal targets were actually present nearby. For most samples, the magnitude of the residual is noticeably smaller than the response indicating that the sample fits the soil model well.

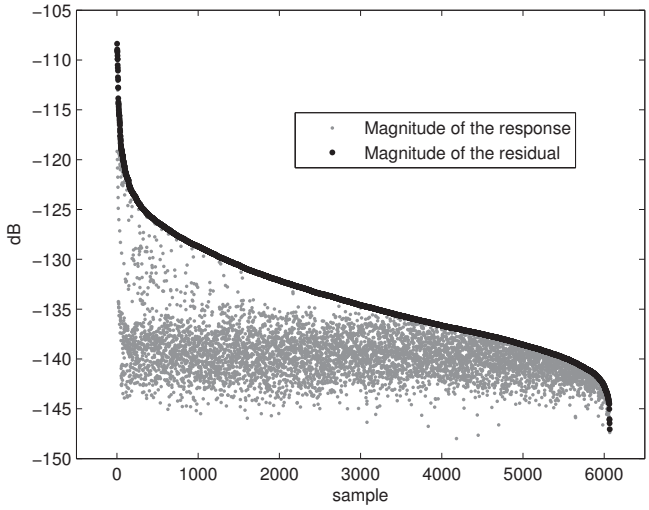

Fig. 2. Samples of blank responses fitted to the soil model (4). The samples are ordered so that response decreases with increasing sample number.

Because the model describes a behavior very specific to the soil and is not usually observed in metallic objects, the model can be used as a prescreener to determine whether a target is present based on the fitting residual. Given a frequency response $H(\omega)$, the response is fitted to (4), and then the residual of the fit ϵ is used to determine whether a metallic object is present. A threshold θ is chosen to decide whether a metallic object is present:

$$\text{target present} = \begin{cases} \text{true} & \text{if } \epsilon > \theta \\ \text{false} & \text{otherwise.} \end{cases} \qquad (5)$$

A reasonable choice of θ for our measurement is -135 dB, as suggested by Fig. 2.

2.3. Detection Framework

A detection framework that incorporates the soil prescreener and the target classifier is presented here. The framework is designed to be suitable for practical application where measurements are obtained sequentially in real-time. It is designed according to the scenario where a detection vehicle carrying the EMI sensors is driven forward and EMI responses $\boldsymbol{h}_n$ are collected sequentially.

The prescreener first screens out the responses that are absent of metallic objects. Responses that pass the prescreener (indicating a target is present) are then processed to estimate their DSRFs. Based on the estimated DSRF, the classifier then labels the responses as landmine or not-landmine.

The use of the prescreener significantly reduces the amount of data processed by the DSRF estimator and the target classifier. Because the prescreener takes very little computation time compared to the estimator and the classifier, the average computation time is also greatly reduced by using the prescreener.

A simple voting mechanism is employed to discourage temporary mislabeling of landmines by taking advantage of the sequential measurements. As the detection vehicle passes over the target, often multiple measurement are collected consecutively for that target. In this case, multiple labels x_i are produced, and a more confident decision can be made based on the recent labels. We determine that a landmine is present only when p out of the past q labels are marked as landmine. The voting rule reduces false-alarm rate and increases the confidence level.

The proposed framework is summarized as follows:

Detection Framework

Input: $\boldsymbol{h}_n$, θ , p, $x_{n-q+1} \ldots x_{n-1}$
Output: decision$_n$

Fit $\boldsymbol{h}_n$ to soil model (4) and obtain residual ϵ.
if $\epsilon < \theta$ **then**
    $x_n = 0$
else
    $\hat{S}$ = estimated DSRF of $\boldsymbol{h}_n$
    x_n = classify($\hat{S}$) (0 or 1)
if $\sum_{i=n-q+1}^{n} x_i > p$ **then**
    decision$_n$ = 1
else
    decision$_n$ = 0
return decision$_n$

3. PERFORMANCE

The proposed method is applied on a data set acquired from a testing field that contains 62 types of targets, including 26 types of landmines as well as various types of metallic and nonmetallic clutter. The testing field is divided in to 11 lanes each lane containing 20 grid cells; there are 220 grid cells total. About 145 EMI responses are collected per grid cell. In total, 32,148 responses are collected for the whole field. The acquisition hardware used is described in [11].

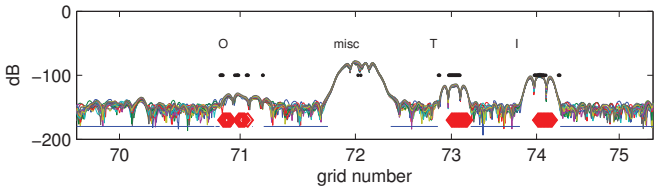

Fig. 3. A snapshot of the output of the detection framework. The curved lines are the strength of the responses measured at 21 frequencies. The target types are noted above the grid number. The blue lines (near -200 dB) indicate points that are marked as soil; black dots (at -100 dB) indicate points that are labeled as landmines; red diamonds indicate a declaration of landmine.

The EMI responses are collected sequentially as the detection vehicle is driven down the lane, and the responses are fed into the detection framework described earlier. The parameters are chosen such that $p = 5$, $q = 20$, and $\theta = -135$ dB. A snapshot of the output of the framework is shown in Fig. 3. Because the way the responses are filtered [11], a target response has multiple lobes (e.g., grid 71 to 74), and only the main (center) lobe is used for processing. The center lobe is determined by the sign of the strongest imaginary part of the response.

In Fig. 3, we see that the soil prescreener is quite effective and the voting rule reduces false alarms. In grid 72, a miscellaneous clutter is labeled as a landmine for a few times, but because the number of mislabeling is small ($< p$), a landmine is not declared and a false alarm is avoided.

The performance of the detection framework using the SVM is summarized in Fig. 4. The receiver operating characteristic (ROC) curve achieves a high detection rate of 0.96 at a low false-alarm rate of 0.10. Other operating points also provide satisfactory performances.

The detection process takes little computer time. With a single pre-trained SVM, the whole test field (32,148 responses) can be classified using the above process (including estimating the DSRF) in 30 seconds on a 2.66 GHz CPU with 960 MB RAM.

The performance of the detection framework using the kNN is also shown in Fig. 4. The performance is comparable to that of the SVM. However, the processing time is much longer (10+ minutes) due to the many distance computations required to find the nearest neighbor per measurement. While the kNN may not be suitable for real-time application, it is quite robust when sufficient training data are available, as is the case here. When the training data is scarce, the SVM is likely to have smaller generalization error.

The classifiers are trained per grid using a leave-one-out

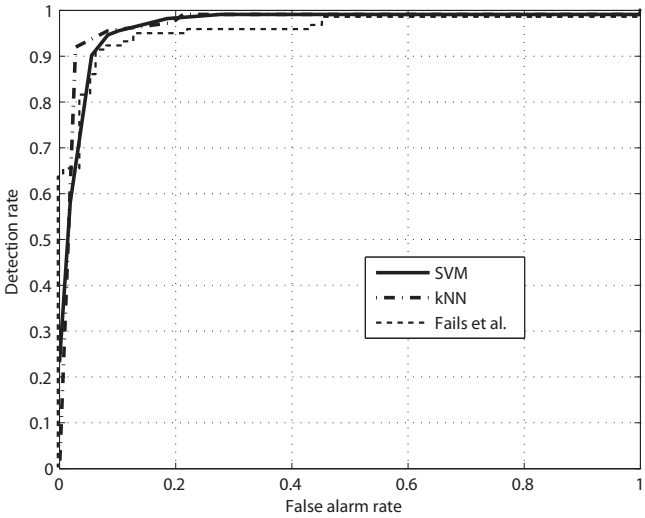

Fig. 4. ROC curves of the proposed method and that of Fails *et al.* [2]. For the kNN ROC curve, $k = 7$.

cross-validation (LOOCV), i.e., the classifiers are trained at each grid with responses from the other 119 grids. Only the strongest responses in a grid are used for training.

For comparison, Fig. 4 includes the ROC curve for the method of Fails *et al.* [2] where the performance is evaluated on the same data set using LOOCV. While the proposed method is slightly better, we note that the simulation done by Fails *et al.* is different from ours. Their method does not utilize sequential measurements.

We note that all the ROC curves in Fig. 4 saturate at 0.99 detection rate. This is due to the misclassification of one particular landmine. Upon close examination, we found that the response of this landmine is very weak and is indistinguishable from the soil response. In our framework, this target is filtered out by the prescreener.

More research can be done to further improve the performance. Other features, such as the soil response and the magnetic property of targets, may be included to provide even more robust performance. Here we only demonstrate the strong potential of using the DSRF for landmine detection.

4. ACKNOWLEDGMENT

This work is supported in part by the US Army REDCOM CERDEC Night Vision and Electronic Sensors Directorate, Science and Technology Division, Countermine Branch and in part by the U. S. Army Research Office.

5. REFERENCES

[1] P. Gao, L. Collins, P. M. Garber, N. Geng, and L. Carin, "Classification of landmine-like metal targets using wideband electromagnetic induction," *IEEE Trans. Geosci. Remote Sens.*, vol. 38, no. 3, pp. 1352–1361, May 2000.

[2] E. B. Fails, P. A. Torrione, W. R. Scott, Jr., and L. M. Collins, "Performance of a four parameter model for modeling landmine signatures in frequency domain wideband electromagnetic induction detection systems," in *Proc. SPIE*, 2007.

[3] G. Ramachandran, P. D. Gader, and J. N. Wilson, "Granma: Gradient angle model algorithm on wideband EMI data for land-mine detection," *IEEE Geosci. Remote Sens. Lett.*, vol. 7, no. 3, pp. 535–539, 2010.

[4] J. T. Miller, T. H. Bell, J. Soukup, and D. Keiswetter, "Simple phenomenological models for wideband frequency-domain electromagnetic induction," *IEEE Trans. Geosci. Remote Sens.*, vol. 39, no. 6, pp. 1294–1298, June 2001.

[5] C. E. Baum, "On the singularity expansion method for the solution of electromagnetic interaction problems," Interaction Notes 88, Air Force Weapons Laboratory, 1971.

[6] M. H. Wei, W. R. Scott, Jr., and J. H. McClellan, "Robust estimation of the discrete spectrum of relaxations for electromagnetic induction responses," *IEEE Trans. Geosci. Remote Sens.*, vol. 48, no. 3, pp. 1169–1179, Mar. 2010.

[7] M. Wei, W. R. Scott, Jr., and J. H. McClellan, "Estimation of the discrete spectrum of relaxations for electromagnetic induction responses using ℓ_p-regularized least squares for $0 \leq p \leq 1$," *IEEE Geosci. Remote Sens. Lett.*, vol. 8, no. 2, pp. 233–237, Mar. 2011.

[8] Y. Rubner, C. Tomasi, and L. J. Guibas, "A metric for distributions with applications to image databases," in *Proc. ICCV*, Bombay, India, Jan. 1998, pp. 59–66.

[9] O. Chapelle, P. Haffner, and V. N. Vapnik, "Support vector machines for histogram-based image classification," *IEEE Trans. Neural Netw.*, vol. 10, no. 5, pp. 1055–1064, 2002.

[10] J. Zhang, M. Marszalek, S. Lazebnik, and C. Schmid, "Local features and kernels for classification of texture and object categories: A comprehensive study," in *CVPRW*, New York, 2006.

[11] W. R. Scott, Jr., "Broadband array of electromagnetic induction sensors for detecting buried landmines," in *Proc. IGARSS*, Boston, MA, July 2008.

[12] Y. Das, "Effects of magnetic soil on metal detectors: preliminary experimental results," in *Proc. SPIE*, New York, 2007, vol. 6553, p. 655306.